2009

Cooling Performance of Arrays of Vibrating Cantilevers

M. L. Kimber

S V. Garimella
Purdue University, sureshg@purdue.edu

Cooling Performance of Arrays of Vibrating Cantilevers

Mark Kimber

Suresh V. Garimella[1]
e-mail: sureshg@purdue.edu

NSF Cooling Technologies Research Center,
School of Mechanical Engineering,
Purdue University,
585 Purdue Mall,
West Lafayette, IN 47907-2088

Piezoelectric fans are vibrating cantilevers actuated by a piezoelectric material and can provide heat transfer enhancement while consuming little power. Past research has focused on feasibility and performance characterization of a single fan, while arrays of such fans, which have important practical applications, have not been widely studied. This paper investigates the heat transfer achieved using arrays of cantilevers vibrating in their first resonant mode. This is accomplished by determining the local convection coefficients due to the two piezoelectric fans mounted near a constant heat flux surface using infrared thermal imaging. The heat transfer performance is quantified over a wide range of operating conditions, including vibration amplitude (7.5–10 mm), distance from heat source (0.01–2 times the fan amplitude), and pitch between fans (0.5–4 times the amplitude). The convection patterns observed are strongly dependent on the fan pitch, with the behavior resembling a single fan for small fan pitch and two isolated fans at a large pitch. The area-averaged thermal performance of the fan array is superior to that of a single fan, and correlations are developed to describe this enhancement in terms of the governing parameters. The best thermal performance is obtained when the fan pitch is 1.5 times its vibration amplitude. [DOI: 10.1115/1.3153579]

Keywords: local heat transfer, piezoelectric fan, fan array, electronics cooling, vibrating cantilever, heat transfer enhancement

1 Introduction

A piezoelectric fan is a cantilever beam whose vibration is actuated by means of a piezoelectric element. This element is typically bonded near the clamped end of the beam and induces a bending moment at the interface between the cantilever beam and the piezo element when a voltage is applied. For an alternating voltage, the beam is set into an oscillatory motion, which in turn creates motion in the surrounding fluid. This fluid motion has been shown to provide heat transfer enhancements with low power consumption in an otherwise quiescent region. These devices can also be configured to meet the geometric constraints of applications where the limited available volume might preclude the use of traditional cooling techniques. The fan design can be tailored to operate at frequencies, which are inaudible to the human ear. Due to these attractive features, piezoelectric fans have been investigated in the literature for practical cooling applications.

Vibrating cantilever-type structures have been commonplace in engineering for decades. However, detailed studies of the motion induced in the surrounding fluid, and more importantly its effect on heat transfer, have only been recently undertaken. Flow field measurements around a cantilever vibrating in quiescent air at relatively small vibration amplitudes (less than 3 mm peak-to-peak tip vibration) were obtained by Kim et al. [1]. They observed a pair of counter-rotating vortices from each oscillation cycle. These vortices were shed from the fan tip as it passed the position of zero displacement. The maximum velocity occurred in the region between these two vortices and just beyond the cantilever tip, and was measured to be approximately four times the maximum tip velocity. Kimber et al. [2] experimentally measured the local heat transfer characteristics of piezoelectric fans and developed heat transfer correlations based on applicable dimensionless numbers.

Numerical modeling of the fluid flow and heat transfer induced by a piezoelectric fan was also conducted [3]. The flow field generated by these fans was found to be extremely complex and highly dependent on the distance from the fan tip to the heat source, as well as other boundary conditions. A single piezoelectric fan vibrating near a small heat source was also experimentally investigated to determine the conditions under which the average heat transfer could be optimized. The factors considered were fan length, vibration amplitude, frequency offset, and distance from the heat source. Optimal conditions occurred when the fan operated at resonance and was oriented normal to the heat source. Under these conditions, an enhancement of over 375% in the heat transfer coefficient was obtained when compared with natural convection alone.

A number of studies have demonstrated the potential of these fans as cooling solutions and explored implementation and feasibility issues [4–7]. Most of these studies have considered single fans, and a more complete review of the literature is available in Ref. [2]. The present work considers the practically important configuration in which multiple fans are used in arrays, and where the complexity increases substantially in describing the structural, fluidic, and heat transfer behavior.

The two-dimensional flow field generated from two flexible cantilevers was analyzed experimentally by Ihara and Watanabe [8]. They investigated the behavior for in-phase and out-of-phase vibration at three different pitches. The cantilevers were sandwiched between two large plates, thereby approximating a two-dimensional flow field. The results were compared with the flow field generated by a single cantilever in the same experimental setup, and the volumetric flow rate for in-phase vibration of two cantilevers was found to be approximately double that of a single cantilever. Pumping capabilities of an array of vibrating beams were analyzed by Linderman et al. [9]. Flow rates produced by micromachined cantilevers in a channel were measured for both a single cantilever and a linear array of cantilevers. The flow rate for the single cantilever varied linearly with frequency, length, and vibration amplitude. Three fans placed in series resulted in a nearly tripled flow rate. The fan pitch was not considered as a variable, and the interaction between neighboring fans was not captured. Mass transfer measurements were obtained by Schmidt
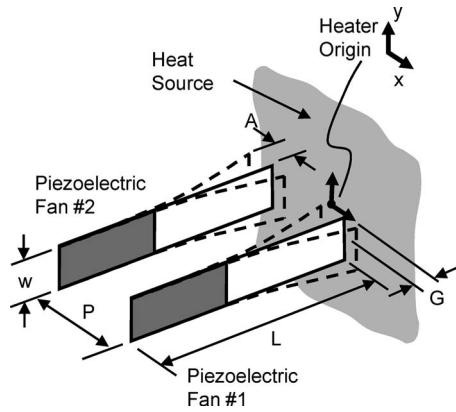
Fig. 1 Experimental parameters: vibration amplitude (A), gap from heat source (G), and fan pitch (P). Also shown is the piezoelectric fan length (L) and width (w).

[10] on a vertical surface mounted near two piezoelectric fans. The fan blades vibrated out of phase and the fan pitch was kept constant. Power-law correlations were found to reasonably describe both maximum and surface-averaged Sherwood numbers for three different distances from the vertical surface. In each case the Sherwood numbers formed contours that were symmetric about the midpoint of fan separation.

Changes in fan vibration parameters influence the flow field and heat transfer performance. A number of studies [11–13] have shown that the vibration characteristics of a vibrating cantilever are altered by the presence of a second oscillating beam. Hosaka and Itao [11] and Basak and Raman [12] showed that fluidic loading on an array of vibrating beams is greatly altered depending on the vibration amplitude as well as the pitch and phase difference between neighboring cantilevers. This was confirmed experimentally by Kimber et al. [13] who observed fluidic coupling between multiple piezoelectric fans. They measured resonance frequency and quality factors for fans vibrating in air and observed a decrease in viscous drag when the fans vibrated in phase, which allowed the fans to achieve larger vibration amplitudes for a given input signal relative to a single fan.

In the present work, local and area-averaged heat transfer characteristics of arrays of piezoelectric fans are investigated. This work follows previous work by the authors [2] in which the thermal performance of a single fan was studied in detail. Of particular interest in this work is the increase in performance obtained with the addition of a second fan, as well as the coupling conditions under which the overall heat transfer rate can be maximized.

2 Experimental Setup and Procedures

The experiments in this work are performed using the setup and procedures described in Ref. [2] and only salient details are provided here.

2.1 Experimental Setup. A flat constant heat flux surface is mounted in a vertical position on an optical table and coated on both sides with a thin layer of Krylon 1602 black paint having a known emissivity of 0.95 [14]. Positioned normal to this surface are piezoelectric fans on two linear stages. This fan orientation with respect to the heater is identical to that used in Ref. [2] and is illustrated in Fig. 1. One linear stage controls the distance from the fan tip to the heated surface, while the other controls the separation between the fans or the pitch. The side of the heated surface opposite the fans is also exposed to ambient conditions and provides access for the infrared camera (ThermaCAM Merlin) with which full-field temperature measurements are captured, thereby enabling convection coefficients to be computed on a point-by-point basis. Two laser displacement sensors (Keyence LK-G157) are positioned near the fan tip to capture the vibration

amplitude for each fan independently. Only in-phase vibration is considered based on past results [8,13], which suggested that in-phase vibration creates constructive interference within the fluid domain while the opposite is true for out-of-phase vibration. As the resonance frequencies of any two fans cannot be matched exactly, a phase difference exists between their motions even with identical input signals. Therefore, a two-channel phase-controlled function generator (Tektronix AFG3022) is employed to ensure in-phase vibration of the fans in all experiments. A plexiglass enclosure is built around the entire setup to isolate it from extraneous air currents within the laboratory.

The constant-flux heat source design is described in Ref. [2] and consists of an electrically heated thin stainless steel (type 302) foil stretched over two 25.4 mm diameter copper rods acting as busbar terminals. The foil is 0.051 mm thick and 101.6 mm wide. The required potential drop across the copper rods is achieved with a high-current power supply. Spring-loaded bolts are used to accommodate thermal expansion and maintain the heated foil in tension. A 25.4-mm-thick plexiglass frame holds the heater assembly together and also provides electrical isolation between the two ends of the heater. The copper rods are separated by a distance of 203.2 mm, thereby providing a heated surface area of 101.6 × 203.2 mm².

As the thermal conductivity of the copper busbars is much larger than that of the stainless steel, the busbars can act as a local heat sink. This localized cooling effect is experimentally found to be confined to a region close to the busbars; therefore, all the heat transfer results are obtained for the portion of the heated foil remote from the busbars. A span of the foil 25.4 mm in length adjacent to each copper rod is excluded from the analysis, leaving a heated surface area of 101.6 × 152.4 mm² that is considered in the measurements.

2.2 Local Heat Transfer Calculations. The electrically generated heat flux (q''_{gen}) is uniform across the entire heated surface and is computed according to

$$q''_{gen} = \frac{V_s \cdot I_s}{A_{heat}} \tag{1}$$

A local flux balance is employed to determine the convection coefficient due to the piezoelectric fans. Radiation losses (q''_{rad}) occur on both sides of the heater and are quantified from the measured temperature field and known surface emissivity. As losses due to natural convection (q''_{nc}) must also be quantified, a number of experiments are conducted in the absence of fans. Natural convection temperature maps are analyzed at multiple levels of power input to the heat source, thereby yielding the experimental dependency of the natural convection coefficients on position and surface temperature. This information is used during the forced convection experiments to account for natural convection losses present on the side opposite the fans. After subtracting these losses (natural convection and radiation), the remaining component of the heat generated is dissipated as q''_{mixed} by mixed convection with contributions from both forced convection (due to the piezoelectric fans) and natural convection. The relationship in such a regime can be approximated as [15]

$$Nu_{mixed}{}^3 = Nu_{pz}{}^3 + Nu_{nc}{}^3 \tag{2}$$

Taking each of these Nusselt numbers to be based on the same length scale, the convection coefficient attributed to the piezoelectric fan (h_{pz}) can be extracted according to

$$h_{pz} = (h_{mix}{}^3 - h_{nc}{}^3)^{1/3} \tag{3}$$

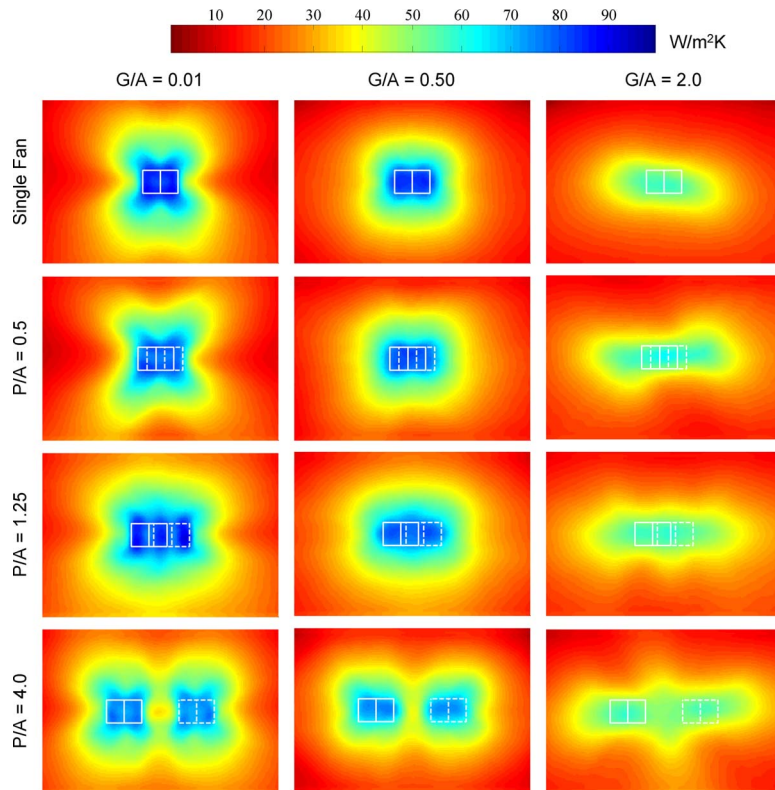where h_{mixed} is directly found from

Fig. 2 Experimental convection coefficient contours (h_{pz}) for $A=10$ mm and $G/A=0.01$ (first column), $G/A=0.50$ (second column), and $G/A=2.0$ (last column). The first row illustrates single-fan performance at the same gaps, while the remaining rows are the results from array experiments with each row representing a different pitch corresponding to P/A $=0.5,1.25,4.0$. The heater size shown is 101.6×152.5 mm^2. Vibration envelopes are superimposed to show location of fans with solid and dashed lines depicting the first and second fans, respectively.

$$h_{\text{mixed}} = \frac{q''_{\text{gen}} - 2 \cdot q''_{\text{rad}} - q''_{\text{nc}}}{T_s - T_\infty} \qquad (4)$$

The convection coefficients reported in the results below exclusively represent the forced convective contribution due to the piezoelectric fans (h_{pz}).

2.3 Experimental Parameters. The commercially available fans used in the experiments are made from a flexible Mylar blade. As shown in Fig. 1, the overall fan length (L) is 64.0 mm, the width (w) is 12.7 mm, and the fundamental resonance frequency of the fan is 60 Hz, which is used as the excitation frequency for all experiments. Also illustrated in the figure are the experimental parameters: vibration amplitude (A), which is half the peak-to-peak amplitude, pitch (P), and gap (G) from the fan tip to the heated surface. To explore the effect of each of these parameters on the heat transfer performance, multiple values of each are considered. Three amplitudes of vibration are investigated ($A=7.5$, 8.5, and 10 mm) and are achieved by adjusting the magnitude of the input voltage signal until the desired amplitude is reached. It should be noted that this adjustment is also dependent on the proximity of the second fan, as well as the distance of the fans from the heated surface. These separation distances govern the viscous drag, an increase or decrease in which causes the amplitude to change significantly [13]. As the viscous drag is reduced for fans vibrating in phase, this can result in a large increase (30%) in vibration amplitude without the need for additional input power. The current investigation, however, is aimed at the underlying physics responsible for heat transfer. Thus, comparisons are made for specified amplitudes, rather than for given

input signal voltages. It should be noted that the total power consumption for the two-fan configuration at a particular amplitude is generally less than double to that needed for a single isolated fan. For example, the total power consumption ranges from 27 mW to 44 mW for the array, whereas the corresponding single fan power consumption is approximately 22 mW for the largest amplitude ($A=10$ mm). The remaining two parameters varied in the experiments (gap and pitch) are expressed as dimensionless quantities normalized by the vibration amplitude. They range from 0.01 to 2.0 and 0.5 to 4.0 for G/A and P/A, respectively. The uncertainty associated with the determination of convection coefficients was estimated in Ref. [2] and is approximately ±8%.

3 Results and Discussion

In this section, the experimental results for local convection coefficients are presented, followed by an analysis of the stagnation and area-averaged heat transfer rates. Comparison is made to a single fan to illustrate the relative performance of arrays of fans.

3.1 Distribution of Local Convection Coefficients. Determination of the forced convection coefficient due exclusively to the piezoelectric fans requires a thorough analysis of the setup in natural convection conditions. Full details of natural convection experiments using this setup can be found in Ref. [2] and are not repeated here; the measured natural convection coefficients were found to be in satisfactory agreement with predictions from established correlations [16] for natural convection from a vertical constant flux heat source. Local forced convection coefficient (h_{pz}) maps are presented in Fig. 2; the same scale is used in all the

images to enable direct qualitative and quantitative comparison between the different cases. Each column represents a change in gap ranging from small ($G/A=0.01$) to large ($G/A=2$) gaps from left to right. Maps of single-fan experiments from Ref. [2] are reproduced as the first row in Fig. 2 to further facilitate comparison. For the three images in the first row, the fan is located at the center of the heat source and the vibration envelope is superimposed. The solid vertical line in the center of the vibration envelope represents the fan at its zero (undisplaced) position, while the remaining lines trace the extent of the vibration envelope whose overall dimensions are twice the vibration amplitude in the horizontal direction and equal to the width of the fan in the vertical direction. The heater size for all images in Fig. 2 is 101.6 $\times$ 152.4 mm^2.

For a single fan, a lobed pattern is generated when the fan vibrates close to the surface; these lobes appear to be symmetric in both the vertical and horizontal directions, suggesting that the fluid agitation is roughly similar in the vibration direction, as well as its orthogonal direction. This behavior transitions to a nearly circular (or rounded-square) shape for the intermediate gaps, while the largest gap results in elliptical contours. The cooling effect is felt over a larger area in the horizontal direction in contrast to the somewhat localized behavior seen at small gaps. Although the magnitude of the heat transfer coefficients is lower for the largest gap, the horizontal extent over which the influence of the fan is felt is greater.

The remaining three rows in Fig. 2 are nine unique cases selected from the experiments conducted when a second fan is present, with each row representing a different pitch. The vibration envelopes of the two fans are illustrated with solid and dashed lines for the first and second fans, respectively. In-phase vibration allows overlapping vibration envelopes, as in the case of small or intermediate pitch (rows 2 and 3 of Fig. 2). The results for the smallest pitch ($P/A=0.5$, second row of Fig. 2) exhibit remarkably similar trends to those observed over the range of gaps for a single fan. In particular, when the fans are located close to the heated surface ($G/A=0.01$), a lobed pattern is once again realized. This pattern transitions to circular and eventually to a somewhat elliptical pattern. One difference that may be noted is the lower magnitude of the convection coefficients for these cases compared with their single-fan counterparts. For a small gap, this suggests that adding a second fan at such a small pitch has a mildly negative effect on the overall performance. However, the opposite appears to be the case for large gaps as seen in the last column of Fig. 2, where the magnitude is quite comparable to that of a single fan but the horizontal coverage has now increased.

As the fan pitch is increased to $P/A=1.25$ (third row of Fig. 2), the behavior exhibits some notable differences from that of a single fan. For the small gap, there now appear to be three zones of enhanced cooling: two at the extreme horizontal ends of the combined vibration envelope and one at the center of the two fans. This is consistent with the findings in Ref. [8], where constructive interference was observed under certain conditions for two cantilevers vibrating in phase. A similar trend can also be seen at the largest gap ($G/A=2$), where the elliptical contours also show enhanced cooling in these three zones.

Maps for the largest pitch ($P/A=4$) are shown in the last row of Fig. 2. Contours at the small gap reveal regions where the behavior is similar to two isolated fans, yielding four distinct lobes surrounding each vibration envelope. However, the convection coefficients are somewhat reduced when compared with a single fan at the same gap. In the limit of a sufficiently large fan pitch, two separate sets of contours identical to single-fan behavior would be expected, but it is apparent from the results that this condition is not fully satisfied for $P/A=4$. Although the contours are similar, the presence of the second fan causes the overall performance to decrease; the same is observed for the intermediate gap ($G/A=0.5$). A possible reason for this behavior is discussed in more detail at the end of this section. The largest gap ($G/A=2$) does not

seem to share these characteristics, and the additional region of cooling between the fans has become more pronounced. It is also interesting to note the similarities between the $G/A=2$ maps at the different fan pitches (far right column of Fig. 2). The general shape and magnitude of the convection coefficient maps are similar, regardless of pitch. This is an important consideration for actual implementation of these fans in arrays. The performance decreases as the gap increases, but a greater fan pitch can be used under these conditions without sacrificing any additional performance; this implies that a smaller number of fans can be used in an array under these conditions.

To facilitate a quantitative analysis of the important trends, convection coefficients are presented along the horizontal centerline of the heat source ($y=0$) in Fig. 3 for a number of gaps and four different pitches. In each case, corresponding profiles for a single fan ($G/A=0.01$) and for natural convection alone (in the absence of fan operation) are also shown for comparison; the vibration envelopes are illustrated by vertical solid and dashed lines for the first and second fans, respectively. Profiles for $P/A=0.5$ are shown in Fig. 3(a), which again illustrates the decrease in performance of a fan array compared with a single fan. However, it is interesting to note that the profiles for all gaps less than $G/A=1$ are nearly identical in the stagnation region. Two fans at this pitch appear to be insensitive to relatively large changes in gap (up to G/A of 1).

An increase in pitch to $P/A=1$ in Fig. 3(b) reveals the constructive interference previously mentioned. Compared with a single fan, the stagnation performance has increased by over 10%, and for the three smallest gaps shown is roughly constant over a large portion of the combined vibration envelope of both fans. A further increase in pitch (to $P/A=1.25$, Fig. 3(c)) shows the three zones of enhanced cooling. This is most apparent for G/A less than 0.25, but the effect persists at $G/A=0.5$. As the gap is increased to $G/A=2$, the shape and magnitude of the profile approach the results seen at this same gap and smaller pitch ($G/A=2$ and $P/A=0.5$ of Fig. 3(a)).

For the largest pitch considered ($P/A=4$, Fig. 3(d)), the profiles start to take the general shape of two isolated fans. However, as previously mentioned, the magnitude of the convection coefficients is somewhat lower when compared with that from the single fan, suggesting that truly isolated conditions are not achieved at $P/A=4$. Additional experiments conducted at larger pitches not covered in Fig. 3 yielded profiles with magnitudes approaching that of a single fan as expected, but the size of the experimental heat source prevented a pitch large enough to yield completely isolated conditions. The observed decrease in performance of two fans relative to a single fan could be attributed localized "trapping" of heated air close to the heat source in the case of the two fans. The ambient temperature in the test setup is measured approximately 10 cm from the heat source, and localized increases in air temperature near the surface are not captured in the ambient temperature measurement.

3.2 Stagnation and Area-Averaged Heat Transfer Coefficients. Correlations for the area-averaged heat transfer for a single fan were presented in an earlier study [2] in terms of dimensionless quantities involving vibration amplitude and distance from the heat source. The calculation of average heat transfer coefficients depends on the geometry of the heat source over which the averaging is performed. In the case of fan arrays, a rectangular target area is most appropriate for averaging. The applicable dimensionless parameters in this correlation process are first defined, after which the stagnation heat transfer coefficient for fan arrays is considered. The area-averaged heat transfer characteristics of fan arrays are then explored.

3.2.1 Nondimensional Parameters. As discussed in Ref. [2], the length scale employed in the applicable dimensionless numbers is the hydraulic diameter of the vibration envelope given as
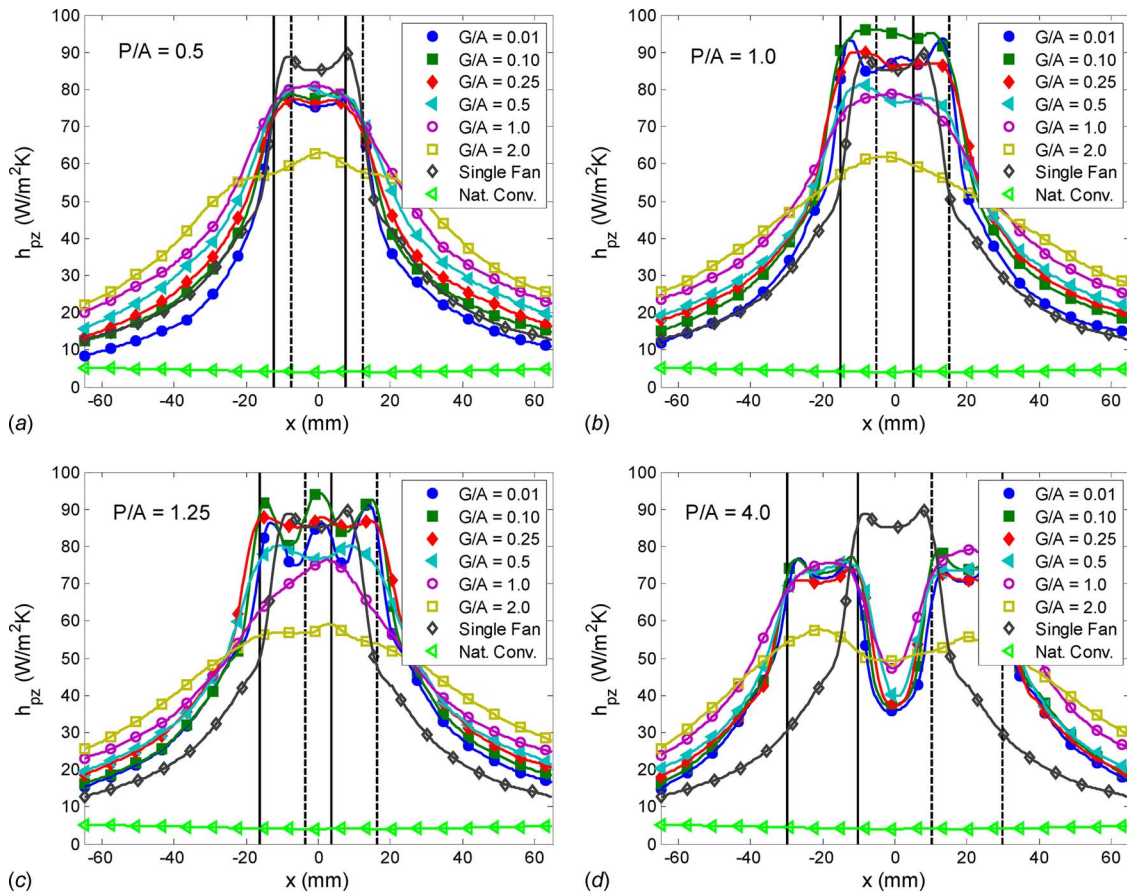
Fig. 3 Convection coefficients (h_{pz}) along the horizontal centerline of the heat source ($y = 0$) over a range of nondimensional gaps ($G/A = 0.01, 0.1, 0.25, 0.5, 1.0, 2.0$) for (a) $P/A = 0.5$, (b) $P/A = 1.0$, (c) $P/A = 1.25$, and (d) $P/A = 4.0$. For comparison, the single-fan ($G/A = 0.01$) and natural convection profiles are also shown. The solid and dashed vertical lines represent the vibration envelopes of the first and second fans, respectively.

$$D_{pz} = \frac{4Aw}{2A + w} \quad (5)$$

The stagnation, local, and area-averaged heat transfer is depicted by Nusselt numbers based on this length scale and the corresponding heat transfer coefficients as follows:

$$Nu_0 = \frac{h_0 \cdot D_{pz}}{k}, \quad Nu = \frac{h_{pz} \cdot D_{pz}}{k}, \quad \overline{Nu} = \frac{\overline{h}_{pz} \cdot D_{pz}}{k} \quad (6)$$

where h_0 is the local convection coefficient at the center of the vibration envelope. The average heat transfer coefficient is dependent on the area of the heat source and can be expressed for an arbitrary geometry as

$$\overline{h}_{pz} = \frac{1}{A_{eq}} \int \int_{A_{eq}} h_{pz} dA_{eq} \quad (7)$$

The influence of vibration amplitude is captured with a piezoelectric fan Reynolds number based on the maximum tip velocity (ωA) and the hydraulic diameter of the vibration envelope according to

$$Re_{pz} = \frac{\omega A D_{pz}}{\nu} \quad (8)$$

3.2.2 Stagnation Nusselt Number for Fan Arrays. The following correlation for stagnation Nusselt number developed in Ref. [2] is independent of heat source geometry and is expected to apply for fan arrays as well

$$Nu_0 = (Re_{pz})^{q_1} \left[C_1 \left(\frac{G}{A} \right)^{q_2} + C_2 \right] \quad (9)$$

Here, $q_1 = 0.440$, $q_2 = 1.451$, $C_1 = -0.168$, and $C_2 = 1.358$. Experimental results for stagnation Nusselt number for the fan array are compared with predictions from this correlation in Fig. 4 for $Re_{pz} = 3640, 2920$, and 2430, corresponding to $A = 10$, 8.5, and 7.5
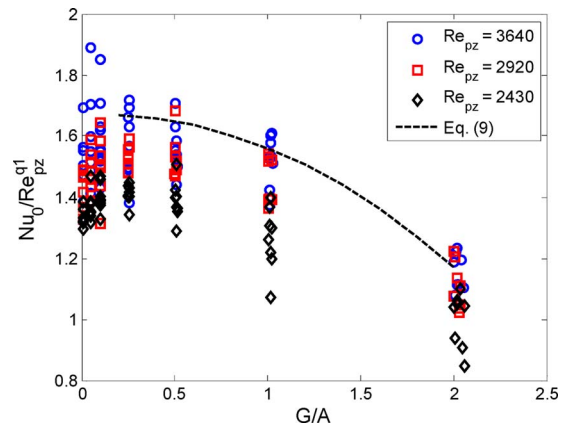

Fig. 4 Stagnation Nusselt number for fan arrays at $Re_{pz} = 3640, 2920$, and 2430 corresponding to $A = 10$, 8.5, and 7.5 mm. These are compared with the single fan correlation in Eq. (9).
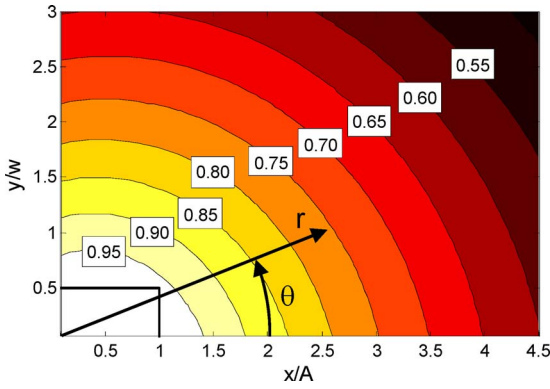
Fig. 5 Map of $\overline{\mathrm{Nu}}/\mathrm{Nu_0}$ (values in boxes) for a single fan from the correlation in Eq. (10). Also illustrated are polar coordinates (r, θ) as defined in Eq. (11).

Fig. 6 Illustration of unit cell area used in computing $\overline{\mathrm{Nu}}$. The horizontal dimension is always equal to half the pitch ($x = P/2$), while the vertical dimension can vary depending on the size of the heat source.

mm, respectively. Data from the largest $\mathrm{Re_{pz}}$ value (3640) agree well with the single-fan correlation but the results diverge as the amplitude (Reynolds number) is decreased. As explained earlier, this deviation is likely due to higher air temperatures near the heater surface for the fan arrays, especially at low fan velocities (low amplitudes) when the heated air is not as effectively transported away. Nonetheless, the single-fan stagnation correlation may be used to estimate stagnation Nusselt numbers in fan arrays to a first approximation.

3.2.3 Area-Averaged Array Nusselt Number. A predictive correlation developed for Nusselt numbers averaged over a circular area in Ref. [2] for a single fan is adjusted here to account for a rectangular averaging area and takes the following form:

$$\overline{\mathrm{Nu}} = \mathrm{Nu_0}(1 + [a(\theta)\exp\{b(\theta)r\}]^{-P(\theta)})^{-1/P(\theta)} \quad (10)$$

where

$$r = \left[\left(\frac{x}{A}\right)^2 + \left(\frac{y}{w}\right)^2\right]^{1/2}, \quad \theta = a\tan\left(\frac{y/w}{x/A}\right) \quad (11)$$

The horizontal and vertical distances that define the heat source geometry are normalized by the vibration amplitude and fan width, respectively. The heat source geometry defined by x/A and y/w was transformed in Eq. (10) to polar coordinates using Eq. (11). The three parameters (a, b, and P) in Eq. (10) are well represented by the following curvefits:

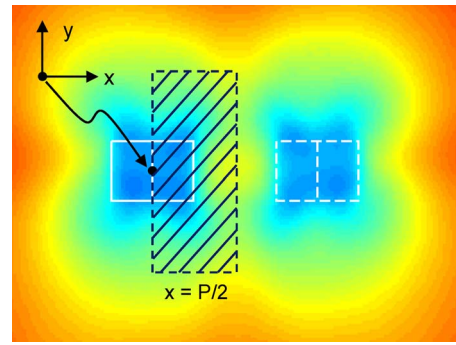$$a(\theta) = 1.181 - 0.054\theta, \quad b(\theta) = -0.150 - 0.017\theta,$$

$$P(\theta) = 39.26 - 6.62\theta \quad (12)$$

The correlation in Eq. (10) yields a two-dimensional map for the normalized Nusselt number ($\overline{\mathrm{Nu}}/\mathrm{Nu_0}$) for a single fan and is shown in Fig. 5. The point $(x/A, y/w)$ of (0, 0) equals the stagnation Nusselt number ($\overline{\mathrm{Nu}}/\mathrm{Nu_0}=1$); other points in the map show $\overline{\mathrm{Nu}}/\mathrm{Nu_0}$ values, which represent the cumulative average from the stagnation point to the $(x/A, y/w)$ at that location (e.g., $\overline{\mathrm{Nu}}$ is approximately half of $\mathrm{Nu_0}$ for $(x/A, y/w)=(4.5, 3)$). It should be noted that the correlation given in Eq. (10) is based on single-fan experiments performed in Ref. [2], but only covers the results for $G/A \leq 0.5$ (unlike the correlation in Ref. [2], which is valid up to $G/A=2$). It is necessary to use the adjusted correlation in order for direct comparison to experimental data from arrays, as explained earlier. The convection contours from an array would repeat from one fan to the next, and therefore a unit cell can be employed to gauge the average thermal performance of the entire array, regardless of the number of fans. This unit cell is illustrated in Fig. 6 and has a horizontal dimension of $x=P/2$ (independent of vibration amplitude). The vertical extent of this unit cell depends on the size of the heat source and is considered a variable in the analysis that follows.

The area-averaged Nusselt numbers for fan arrays are first normalized by their respective experimental stagnation values. The results from $G/A \leq 0.5$ are then averaged for each pitch and compared with the single-fan contours of Fig. 5. A series of constant x/A profiles for a single fan and arrays are shown in Figs. 7(a) and 7(b), respectively. Each curve represents a different value of x/A,
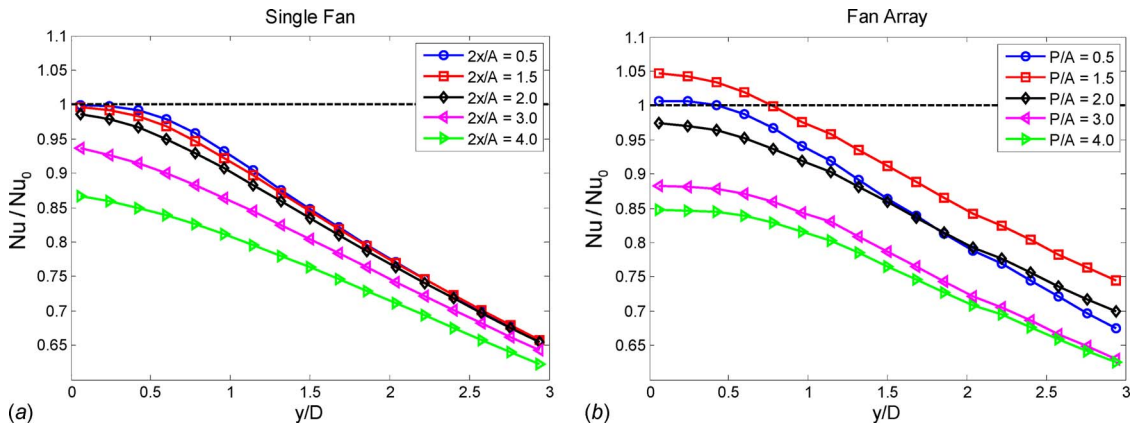

Fig. 7 Profiles of $\overline{\mathrm{Nu}}/\mathrm{Nu_0}$ at different x/A locations: (a) single-fan correlation results from Fig. 5 and (b) experimental array data at the largest amplitude ($\mathrm{Re_{pz}}=3640$). In the case of fan arrays, $2x$ is better represented as P so that the two sets of data correspond to the same area on the heat source.
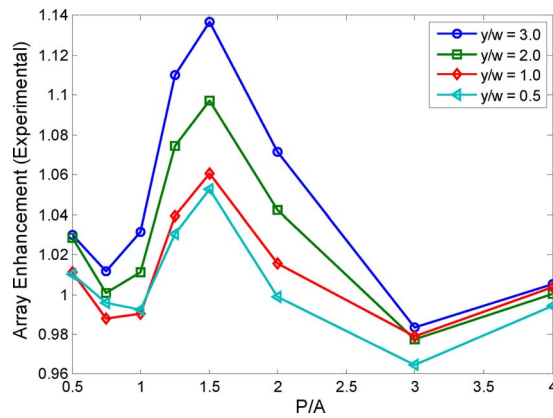
Fig. 8 Experimental enhancement observed with arrays at the largest amplitude ($Re_{pz}=3640$) over the full range of pitches considered. The horizontal dimension of the targeted heat source is $x=P/2$, while the vertical dimension varies with y/w (values of 3.0, 2.0, 1.0, and 0.5 are shown).

Table 1 Correlation coefficients for estimation of array enhancement (Eqs. (13) and (14)). Errors are determined by comparing estimated results with those from Fig. 7 and similar results for smaller amplitudes.

Parameter	Value
C_1	6.12×10^{-3}
C_2	1.5
C_3	1.667
m	1.5
n	1.0
Average deviation	2.5%
Maximum deviation	6.0%

$$Z = \left(\frac{Re_{pz}}{1000} \right)^m \left(\frac{y}{w} \right)^n \qquad (14)$$

with exponents m and n being greater than or equal to unity so that as either variable (Re_{pz} or y/w) increases, the enhancement will also increase.

The variables C_1, C_2, C_3, m, and n are all determined from a least-squares analysis of the data. The results are listed in Table 1 and yield average and maximum errors of 2.5% and 6.0% in accounting for the normalized experimental data. The recommended correlation for heat transfer coefficients with fan arrays is thus the product of Eq. (10) (where Nu_0 is found from the single-fan correlation developed in Ref. [2]) and Eq. (13). The enhancement factor (Eq. (13)) is presented in Fig. 9 for three Re_{pz} values (3640, 2920, and 2430) and two y/w values (3.0 and 0.5).

4 Conclusions

Local heat transfer coefficients are obtained experimentally for arrays of piezoelectric fans and compared with the performance of a single fan. The interaction between neighboring fans is observed in analyzing both the stagnation and area-averaged thermal performance. A modest decrease in stagnation heat transfer for arrays is attributed to an increase in effective ambient temperature, as fans in the array feed heated air to their neighboring fans. For area-averaged results, conditions exist where the heat transfer in fan arrays is enhanced relative to the performance of single fans. The extent of enhancement is found to depend on the vibration amplitude and pitch, as well as the size of the heat source over which the heat transfer coefficient is averaged. Correlations are developed, which describe heat transfer characteristics of fan arrays over a range of operating conditions; a pitch of $P/A=1.5$ yields the largest increase in area-averaged thermal performance
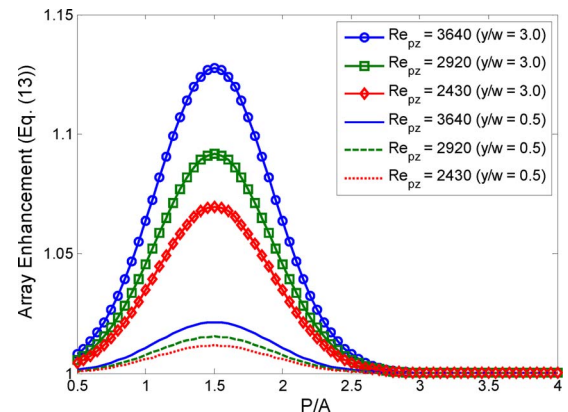
with $P=2x$ shown in the legend for the array curves (Fig. 7(b)). Note that for the curves in Fig. 7(a) with $2x/A \lesssim 2.0$, the average Nusselt number is approximately equal to the stagnation value ($\overline{Nu}/Nu_0=1$) at $y/w=0$, and falls to 65% of the stagnation value ($\overline{Nu}/Nu_0=0.65$) at $y/w=3$. The increase (or decrease) in performance through implementing an array can be found by comparing results from Fig. 7(a) with those from Fig. 7(b). The smallest pitch ($P/A=0.5$) yields little enhancement over its single-fan counterpart ($2x/A=0.5$ in Fig. 7(a)). Likewise, the two largest pitches ($P/A=3, 4$) do not increase the performance over a single fan. In fact, for small y/w values ($y/w<1$), these results suggest a decrease in performance for the array configuration. The most notable difference occurs for the intermediate pitch ($P/A=1.5$), which shows a substantial increase in thermal performance over the entire range of y/w shown. The average Nusselt number in this case is 5% higher than the stagnation value ($\overline{Nu}/Nu_0=1.05$) at $y/w=0$ and falls to 75% of the stagnation value ($\overline{Nu}/Nu_0=0.75$) at $y/w=3$. Therefore, the enhancement in this case over the single fan is 5% for small y/w and 15% ($\overline{Nu}/Nu_0=0.75$ compared with $\overline{Nu}/Nu_0=0.65$) for large y/w.

The enhancement is further illustrated in Fig. 8 for discrete values of y/w and is plotted against fan pitch. The figure reveals an optimum pitch of $P/A=1.5$, with the enhancement dropping off (or becoming negative) for very large or very small pitches. This behavior can be approximated using the following Gaussian-like profile:

$$\text{Enhancement} = \left\{ C_1 Z \exp \left(- \left[\left(\frac{P}{A} - C_2 \right) C_3 \right]^2 \right) \right\} + 1 \qquad (13)$$

In this equation, the function Z represents the dependence of the enhancement factor on the vertical extent of the heat source (y/w) over which the Nusselt number is averaged, as well as on fan amplitude. It should be noted that only results for the largest amplitude ($Re_{pz}=3640$) are included in Figs. 7 and 8. The experimental results from additional amplitudes revealed similar behavior with the optimum pitch in the same range. The observed enhancement is seen to decrease with amplitude, suggesting an additional dependence on Reynolds number. The dependence on these two parameters (y/w and amplitude) is captured with the following power-law relationship:

Fig. 9 Expression for array enhancement over single-fan performance (Eq. (13)) at three amplitudes ($Re_{pz}=3640$, 2920, and 2430) and two values for y/w (3.0 and 0.5)

(approximately 15%) when compared with a single fan. As the pitch becomes smaller or larger, the relative enhancement is found to decrease.

The present study was conducted at prescribed vibration amplitudes for the fans and not at a specified power input to drive the fans. For an array of N fans operating at the optimal pitch, the required power is less than N times the power required for one fan. Therefore, an experiment performed with the input power fixed would yield even further increases in thermal performance than that reported in this work. The optimal value of dimensionless pitch holds true regardless of gap or vibration amplitude and provides a guideline for use in the design of such fan arrays.

Acknowledgment

Nomenclature

A = vibration amplitude (1/2 of peak-to-peak amplitude)
A_{heat} = area of heat source
D_{pz} = hydraulic diameter of vibration envelope
G = gap
h = local convection coefficient
$\bar{h}$ = area-averaged convection coefficient
h_0 = stagnation forced convection coefficient
I_s = current from power supply
k = thermal conductivity
L = piezoelectric fan length
$\underline{Nu}$ = local Nusselt number
$\overline{Nu}$ = area-averaged Nusselt number
Nu_0 = stagnation Nusselt number
P = fan pitch
q'' = heat flux
Re_{pz} = Reynolds number for vibrating cantilever
T_s = surface temperature
T_∞ = ambient temperature
V_s = voltage drop across heater
r = radial location on heat source
w = piezoelectric fan width
x = horizontal location on heat source
y = vertical location on heat source

Greek Symbols

ε = surface emissivity
ν = kinematic viscosity
θ = polar angle from horizontal on heat source
σ = Stefan–Boltzmann constant
ω = vibration frequency

Subscripts

gen = energy generation
mixed = mixed regime convection
nc = natural convection
pz = forced convection (under piezoelectric actuation)
rad = radiation

References

[1] Kim, Y., Wereley, S. T., and Chun, C., 2004, "Phase-Resolved Flow Field Produced by a Vibrating Cantilever Plate Between Two Endplates," Phys. Fluids, **16**(1), pp. 145–162.
[2] Kimber, M., Garimella, S. V., and Raman, A., 2007, "Local Heat Transfer Coefficients Induced by Piezoelectrically Actuated Vibrating Cantilevers," ASME J. Heat Transfer, **129**(9), pp. 1168–1176.
[3] Açıkalın, T., Garimella, S. V., Raman, A., and Petroski, J., 2007, "Characterization and Optimization of the Thermal Performance of Miniature Piezoelectric Fans," Int. J. Heat Fluid Flow, **28**(4), pp. 806–820.
[4] Toda, M., 1979, "Theory of Air Flow Generation by a Resonant Type PVF$_2$ Bimorph Cantilever Vibrator," Ferroelectrics, **22**, pp. 911–918.
[5] Toda, M., 1981, "Voltage-Induced Large Amplitude Bending Device—PVF$_2$ Bimorph—Its Properties and Applications," Ferroelectrics, **32**, pp. 127–133.
[6] Açıkalın, T., Wait, S. M., Garimella, S. V., and Raman, A., 2004, "Experimental Investigation of the Thermal Performance of Piezoelectric Fans," Heat Transfer Eng., **25**(1), pp. 4–14.
[7] Yoo, J. H., Hong, J. I., and Cao, W., 2000, "Piezoelectric Ceramic Bimorph Coupled to Thin Metal Plate as Cooling Fan for Electronic Devices," Sens. Actuators, A, **79**(1), pp. 8–12.
[8] Ihara, A., and Watanabe, H., 1994, "On the Flow Around Flexible Plates, Oscillating With Large Amplitude," J. Fluids Struct., **8**, pp. 601–619.
[9] Linderman, R. J., Nilsen, O., and Bright, V. M., 2005, "Electromechanical and Fluidic Evaluation of the Resonant Microfan Gas Pump and Aerosol Collector," Sens. Actuators, A, **118**(1), pp. 162–170.
[10] Schmidt, R. R., 1994, "Local and Average Transfer Coefficients on a Vertical Surface Due to Convection From a Piezoelectric Fan," International Society Conference on Thermal Phenomena, Washington DC, pp. 41–49.
[11] Hosaka, H., and Itao, K., 2002, "Coupled Vibration of Microcantilever Array Induced by Airflow Force," ASME J. Vibr. Acoust., **124**(1), pp. 26–32.
[12] Basak, S., and Raman, A., 2007, "Hydrodynamic Coupling Between Micromechanical Beams Oscillating in Viscous Fluids," Phys. Fluids, **19**(1), p. 017105.
[13] Kimber, M., Garimella, S. V., and Raman, A., 2006, "An Experimental Study of Fluidic Coupling Between Multiple Piezoelectric Fans," International Society Conference on Thermal Phenomena, San Diego, CA, pp. 333–340.
[14] NASA Jet Propulsion Laboratory Website, http://masterweb.jpl.nasa.gov/reference/paints.htm.
[15] Incropera, F., and DeWitt, D., 2002, *Fundamentals of Heat and Mass Transfer*, 5th ed., Wiley, New York.
[16] Vliet, G. C., and Ross, D. C., 1975, "Turbulent Natural Convection on Upward and Downward Facing Inclined Constant Heat Flux Surfaces," ASME J. Heat Transfer, **97**(4), pp. 549–555.